AIP | Review of Scientific Instruments

Development of 3D microwave imaging reflectometry in LHD (invited)

Y. Nagayama, D. Kuwahara, T. Yoshinaga, Y. Hamada, Y. Kogi et al.

Citation: Rev. Sci. Instrum. **83**, 10E305 (2012); doi: 10.1063/1.4729259

View online: http://dx.doi.org/10.1063/1.4729259

View Table of Contents: http://rsi.aip.org/resource/1/RSINAK/v83/i10

Published by the American Institute of Physics.

Development of 3D microwave imaging reflectometry in LHD (invited)[a)]

Y. Nagayama,[1,b)] D. Kuwahara,[1,2] T. Yoshinaga,[3] Y. Hamada,[1] Y. Kogi,[4] A. Mase,[5] H. Tsuchiya,[1] S. Tsuji-Iio,[2] and S. Yamaguchi[6]
[1]*National Institute for Fusion Science, Toki, Japan*
[2]*Tokyo Institute of Technology, Tokyo, Japan*
[3]*National Defense Academy of Japan, Yokosuka, Japan*
[4]*Fukuoka Institute of Technology, Fukuoka, Japan*
[5]*KASTEC, Kyushu University, Kasuga, Japan*
[6]*Kansai University, Suita, Japan*

(Presented 9 May 2012; received 8 May 2012; accepted 24 May 2012; published online 20 June 2012)

Three-dimensional (3D) microwave imaging reflectometry has been developed in the large helical device to visualize fluctuating reflection surface which is caused by the density fluctuations. The plasma is illuminated by the probe wave with four frequencies, which correspond to four radial positions. The imaging optics makes the image of cut-off surface onto the 2D (7 × 7 channels) horn antenna mixer arrays. Multi-channel receivers have been also developed using micro-strip-line technology to handle many channels at reasonable cost. This system is first applied to observe the edge harmonic oscillation (EHO), which is an MHD mode with many harmonics that appears in the edge plasma. A narrow structure along field lines is observed during EHO. © *2012 American Institute of Physics*. [http://dx.doi.org/10.1063/1.4729259]

I. INTRODUCTION

It is considered that thermal conduction and particle diffusion are governed by turbulences. In high β plasmas, localized modes such as the ballooning mode[1] causes destructive effects on the plasma confinement. Visualization of local electron density fluctuations would be very useful to study the physics of confinement and instabilities in fusion plasma. The local electron density fluctuation can be visualized with microwave. Plasma reflects the X-mode microwave at the cutoff frequency that is

$$\frac{\omega_R}{2\pi} = \frac{1}{4\pi}\left\{\omega_{ce} + \left(\omega_{ce}^2 + 4\omega_{pe}^2\right)^{1/2}\right\} \quad (1)$$

where

$$\frac{\omega_{pe}}{2\pi}\,[\mathrm{GHz}] = 28.4(n_e\,[10^{19}\mathrm{m}^{-3}])^{1/2} \quad (2)$$

and

$$\frac{\omega_{ce}}{2\pi}\,[\mathrm{GHz}] = 28B\,[\mathrm{T}] \quad (3)$$

The O-mode microwave is also reflected at the cutoff frequency of $\omega_{pe}/2\pi$. The microwave imaging reflectometry (MIR) is a device to visualize fluctuating reflection surface which is caused by the density fluctuations.[2]

In the preliminary MIR experiments in the large helical device (LHD),[3–5] reflected microwaves were received with three commercial horn antennas. However, receiver horn were too big to be increased numbers. In early works,[6] the MIR system used a one-dimensional (1D) hybrid-type detector/mixer array, comprised of planar antennas with integrated Schottky diodes. It is hard to make a 2D array of planar antennas, such as bow-tie antenna[7] or dual dipole antenna,[6] because baluns extend from the side of antenna array. A 2D imaging device was firstly used in the MIR experiments[8,9] in the TPE-RX reversed field pinch. In TPE-RX, a stack of four pieces of 1D planar type Yagi-Uda antenna array with mixer diodes[5] were used for the MIR frequency of 20 GHz. In LHD, however, frequencies of microwave diagnostics, such as the electron cyclotron emission (ECE), the X-mode cutoff and the O-mode cutoff frequencies, are much higher as shown in Fig. 1. Planar Yagi-Uda antenna is not useful.

This paper presents the 3D MIR system in LHD. This system consists of 2D microwave imaging device,[10,11] four frequency microwave source,[12] microwave imaging optics with adjustable mirror,[13] and electronics for intermediate frequency (IF) amplification, frequency separation and quadrature detection. By using the 3D MIR, 3D structure of the edge harmonic oscillation (EHO) is observed.

II. IMAGING DEVICE

A stack of seven pieces of 1D horn-antenna mixer array (HMA) is a 2D microwave imaging device that has been developed in LHD. Schematic structure of HMA is shown in Fig. 2. HMA consists of three parts, an upper aluminum frame, a thin printed circuit board (PCB), and a lower aluminum frame. The upper and lower frames have half apertures of pyramidal horn antennas and rectangular waveguide sections. By sandwiching the PCB with the upper and lower frames, a 1D HMA is constructed. The HMA for MIR in LHD is designed for V-band (50–75 GHz). The aperture sizes of each horn and waveguide section of HMA are 13 × 13 mm and 1.9 × 3.8 mm, respectively, and seven small horn apertures are aligned at every 14 mm. The aperture size of

[a)]Invited paper, published as part of the Proceedings of the 19th Topical Conference on High-Temperature Plasma Diagnostics, Monterey, California, May 2012.
[b)]nagayama.yoshio@nifs.ac.jp.

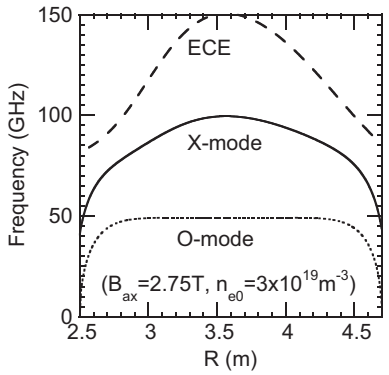

FIG. 1. Frequencies for the electron cyclotron emission (ECE), the X-mode cutoff, and the O-mode cutoff in a typical plasma in LHD.

waveguide section is the same as commercially available V-band (WR15) waveguide. The lengths of horn and waveguide sections are 15.5 mm and 12 mm, respectively. Schottky barrier diodes (SBD) are mounted on the 0.254 mm thick teflon PCB. This is designed as SBD and is set in the middle of waveguide section. SBD mixes the signal wave (RF) and the local oscillation wave (LO), which enter from the horn aperture, and converts to the the intermediate frequency (IF) signal. On the PCB, the obtained IF signals are amplified by monolithic microwave integrated circuits (MMIC).

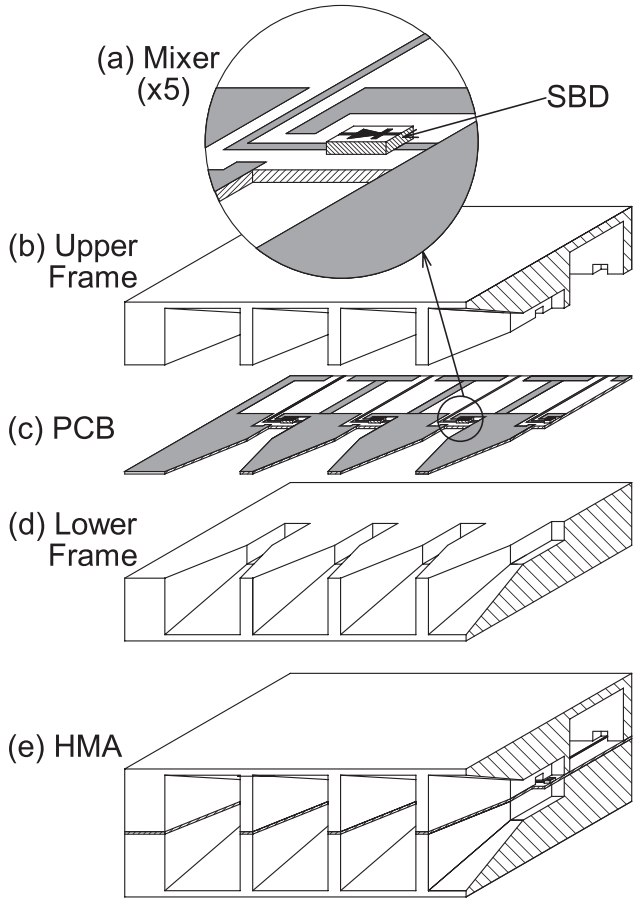

FIG. 2. Schematic structure of HMA.

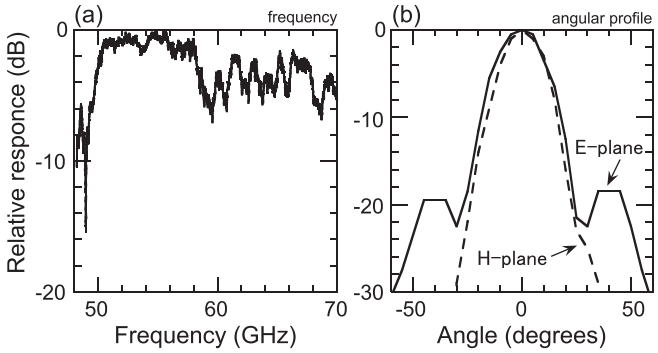

FIG. 3. (a) Frequency response and (b) angular response of HMA.

The frequency and angular responses of the V-band HMA are shown in Fig. 3. In these measurements, the radiated waves from the standard gain horn are received by HMA. The full width at half maximum (FWHM) of the angular response profile is 17° on both H-plane and E-plane. This is wider than that of commercially available pyramid horn which is 10°. The frequency response of HMA is broad. It is confirmed that HMA has a good response between 50 and 109 GHz, but the upper limit is not clear because of the limitation of our measurement system. By stacking the seven seven-channel 1D HMAs, a 2D (7 × 7 channels) imaging device is formed. One array of 1D HMA is dedicated to the ECE imaging, of which frequency region is between 97 and 105 GHz.[14] In LHD, MIR, and ECEI use the same optics and the same HMA. They are dedicated to measure fluctuations of the electron density and the electron temperature at the same plasma position.[15]

III. OPTICAL SYSTEM

The microwave imaging system for LHD is schematically shown in Fig. 4. It is designed that the probe wave

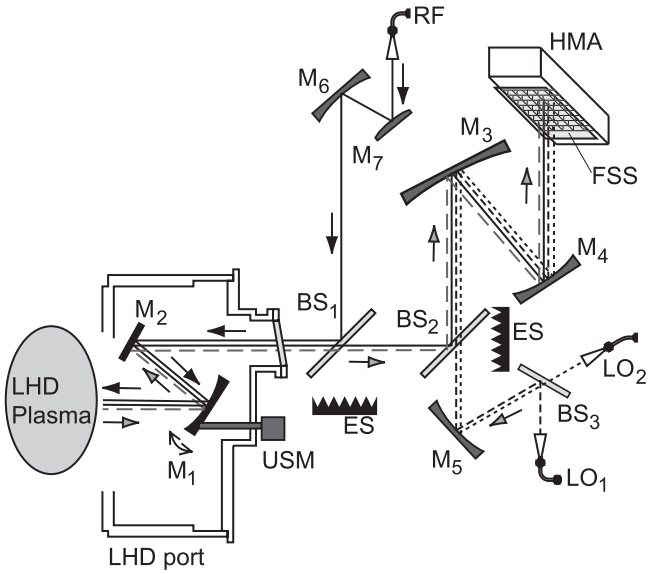

FIG. 4. Schematic diagram of microwave imaging system in LHD. BS_i are beam splitters. ES is ECCOSORB. FSS is a frequency selective surface to reduce 77 GHz. LO_1 and LO_2 are local oscillation waves for MIR and ECEI respectively. M_j are aluminum alloy mirrors.

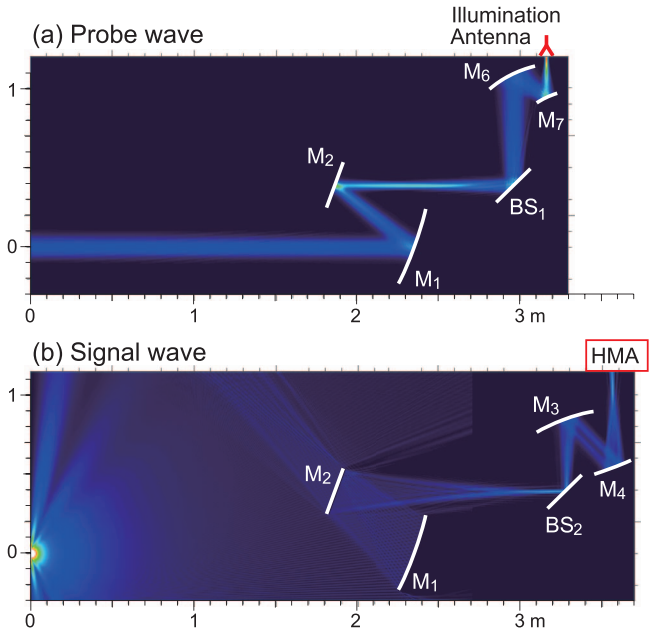

FIG. 5. (a) FDTD simulation of probe wave. (b) FDTD simulation of reflected wave.

illuminates the LHD plasma as a parallel beam. Focal point of the objective ellipsoidal mirror (M_1), of which size is 430 × 500 mm, matches that of the combination optics of a ellipsoidal mirror (M_6) and a hyperboloidal mirror (M_7). The beam diameter is determined by the combination optics. The optical system is also designed to make a plasma image on HMA. A frequency selective surface (FSS)[16] is installed in front of HMA in order to reduce 77 GHz which is the frequency of electron cyclotron heating in LHD. The optical components except mirrors M_1 and M_2, which are installed in the vacuum vessel, are installed on a rigid frame. Angles of the object mirror (M_1) is adjusted in order to maximize the reflection power from the LHD plasma, of which reflection surface is twisted.[4] The LO wave launched from the LO antenna is expanded by a ellipsoidal mirrors (M_3-M_5) illuminates HMA uniformly.

Figures 5(a) and 5(b) show the designed power densities of the probe wave and the signal wave, respectively. This is numerically calculated by using 2D finite-difference time-domain (FDTD) method.[13,17] In the FDTD computation, beam splitters are replaced by a mirror or neglected, while they are thin metal plates with 45° long narrow holes in the experiment. The signal wave from a point in plasma is focused onto the HMA aperture. The image size is determined by ellipsoidal mirrors (M_3, M_4). The size of M_3 is 354 × 390 mm. Figure 6(a) shows power profile of the probe beam, which is measured by a power monitor with a V-band pyramidal horn antenna. The spot size of the probe beam is 20 cm vertically and 15 cm horizontally at $z = 0$ cm, and the spot size varies just a few cm between $z = -40$ and $+40$ cm. Here z is the distance from the focal plane. The illumination wave is a parallel beam with the diameter of 20 cm in the observed region.

The laboratory test of optics including M_1 and M_2 on a test bench is as follows: The probe beam illuminates a target,

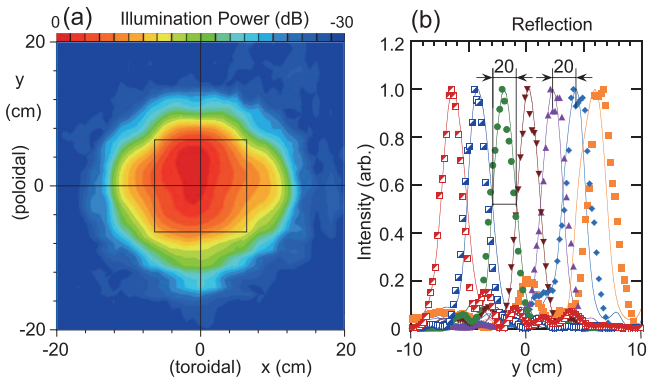

FIG. 6. (a) Power profile of probe wave at the focal plane. (b) Power profiles of reflected wave by the metal rod.

which is a metal rod with the diameter of 10 mm at the plasma position. By scanning the metal rod horizontally or vertically, the scattered wave is received by the HMA to examine the resolution of optics. Figure 6(b) shows the power density profile of scattered wave detected by HMA channels. Channel separation is 20 mm and the resolution is also 20 mm. Measurement and simulation agree well at most channels except few edge channels. Observed plasma area is 140 × 140 mm, and this is uniformly illuminated as is presented in previous report.[13]

Disturbance due to spurious reflections is examined. Figure 7 shows power profiles of reflected wave by the metal rod with a glass window in the laboratory test. When the window is set perpendicular to the beam, the reflected wave by the window masks the signal from the rod. When the window is slanted by 8°, the spurious reflection is decreased about 20 dB and reflected wave by the metal rod can be measured. So, no lens is used in MIR in order to minimize spurious reflections in LHD.

IV. MULTI-FREQUENCY SOURCE AND RECEIVERS

Figure 8 shows schematic diagram of the radio frequency (RF) source and receiver system for MIR in LHD. The frequency source provides the illumination wave with four frequencies ($\omega_{RF}/2\pi$ = 60.41, 61.81, 63.01, 64.61 GHz), the

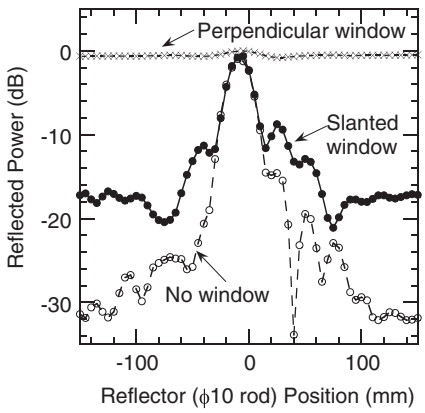

FIG. 7. Power profiles of reflected wave by the metal rod with a glass window on the test bench.

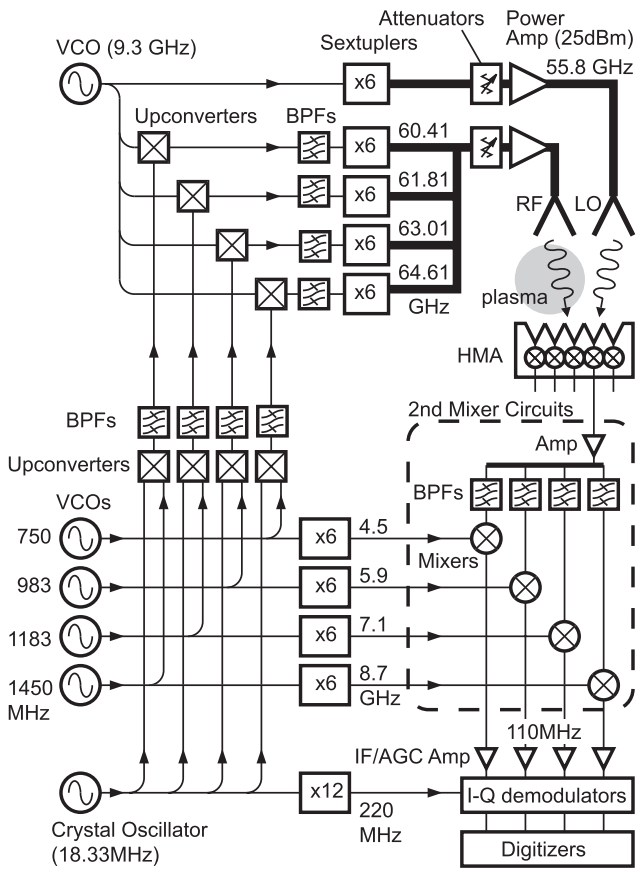

FIG. 8. Four frequencies source and receiver system for MIR in LHD.

LO wave ($\omega_{LO}/2\pi = 55.8$ GHz), references with 4 frequencies ($\omega_{ref}/2\pi = 4.5$, 5.9, 7.1, 8.7 GHz) and the reference ($\omega_{IQ}/2\pi = 220$ MHz) of quadrature demodulators. The carrier wave (9.3 GHz) is generated by a voltage controlled oscillator (VCO). The 1st LO wave (55.8 GHz) is made by sextupling the frequency of the carrier wave and by amplifying up to 25 dBm.

The generation of illumination wave is as follows: First, four frequencies (750, 983, 1183, 1450 GHz) are generated by VCOs. Second, they are separately up-converted with reference frequency (18.33 MHz), which is generated by the crystal oscillator. Upper sideband of each up-converted frequency is taken by a band-pass-filter (BPF) with the band width of 1 MHz. The lower sideband components are reduced by –40 dB by BPFs. Third, each of four up-converted frequencies is separately up-converted with the carrier wave. Again upper sideband of each up-converted frequency is selected by a BPF. Fourth, these four frequencies are separately sextupled and then combined using directional couplers. Finally, the combined wave is amplified up to 25 dBm. Differences of power of four frequencies are within ±2 dB. The LO wave and the illumination wave are transferred by X-band waveguides for 15 m from the source to antennas in the MIR optics. Also the 2nd LO frequencies (4.500, 5.898, 7.098, 8.700 GHz) are generated by sextupling four frequencies (750, 983, 1183, 1450 GHz). The reference frequency (220 MHz) of the quadrature demodulator is made from 18.33 MHz.

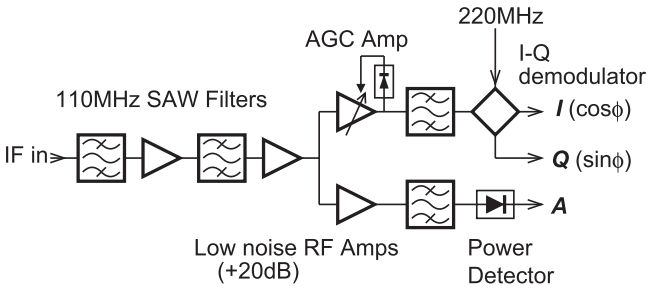

FIG. 9. Block diagram of I-Q demodulation and power detection circuit for MIR.

In the 2D HMA, the reflected wave from plasma and the 1st LO (55.8 GHz) wave are mixed, thus the 1st IF signals are generated. The 1st IF signals are transferred to the 2nd mixer circuits by 15 m coaxial cables. BPFs in the 2nd mixer circuit are made of micro-strip-line technology on a thin Teflon PCB.[5,18] They have the same central frequencies of 2nd LO frequencies and the bandwidth of ~0.3 GHz. In the 2nd mixer circuit, four frequencies are separated by BPFs, and they are mixed with the 2nd LO frequencies. Thus, the 2nd IF signals (110 MHz) are finally obtained. The 2nd IF signals are amplified with MMIC amplifiers and 110 MHz surface acoustic wave (SAW) filters, of which bandwidth is 4 MHz. The intensity and phase of reflected signal are detected with the power detector and the quadrature (I-Q) demodulator, respectively. Block diagram of the signal detection circuit is shown in Fig. 9.

V. EXPERIMENTS

When the electron density is lower than the cutoff density, MIR signal is the wave reflected at the vacuum vessel wall in the inboard side. The phase of reflected wave should be changed due to the refractive index of plasma. Figure 10 shows amplitude (A), in-phase (I), and quadrature (Q) of the MIR signal (63.01 GHz) in the initial stage of the low density plasma with the axial magnetic field of 0.9 T, where the cutoff frequency is much lower than the MIR frequencies. Constant amplitudes of I and Q signal indicate that AGC amplifiers works well. The phase of Q proceeds 90° from I, as $I \propto \cos\phi$ and $Q \propto \sin\phi$. The line integrated electron density is also shown in Fig. 10. From $t = 3.41$ to 3.42 s, nL increases by 0.284×10^{19} m^{-2} and the phase of MIR proceeds 12.3

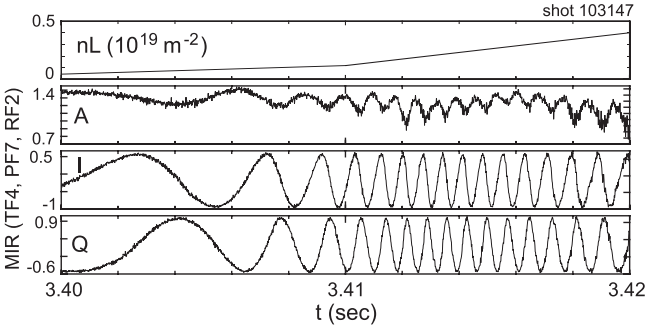

FIG. 10. Raw signal of MIR in the case of low density plasma.

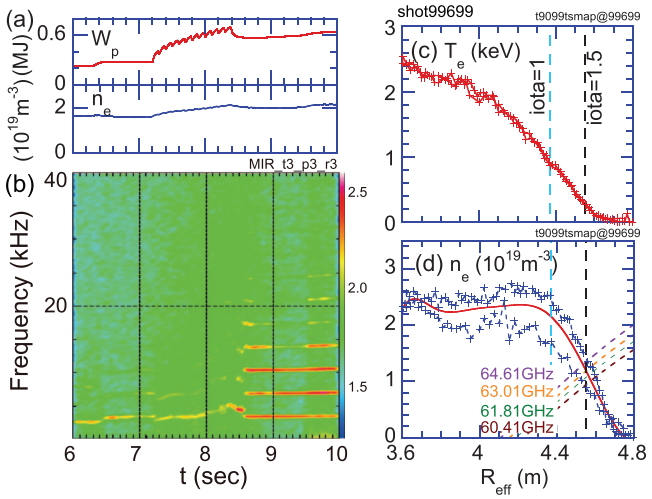

FIG. 11. (a) Time evolution of internal plasma energy, line averaged electron density. (b) FFT spectrum of MIR signal. Profiles of (c) electron temperature and (d) density at t = 9.1 s.

fringes. Suppose probe beam is reflected at the vacuum vessel wall, estimated phase difference for $\Delta nL = 0.284 \times 10^{19}$ m^{-2} is 12.3 fringes, which agrees well to the observation. This data indicates the detection system works well.

By the use of MIR we observe the edge harmonic oscillation (EHO), which appears near the plasma edge and has equally separated many harmonics of the baseband of a few kHz. Edge plasma affects both the heat flux to the plasma facing component and the plasma confinement. In tokamaks, EHO is observed in the quiescent H-mode,[19] where ELM is absent. If EHO enhances particle transport to allow sustained particle control with no change to the edge pressure profile, serious problems due to ELM could be solved by EHO.[20] So EHO would be important phenomena, but EHO has not been well investigated yet.

Figure 11 shows plasma parameters and FFT spectrum of MIR signal when EHO appears. In LHD, EHO appears in medium density plasmas with standard operation without H-mode. At t = 9 s, more than 10 harmonics of the baseband of 3 kHz are observed as shown in Fig. 11(b). The electron temperature and density profiles are shown in Figs. 11(c) and 11(d), respectively. The cutoff densities of probe waves, which are determined with Eq. (1), are also shown in Fig. 11(d). The cross point of curbs of the cutoff and real density may provide the observation point. The plasma edge calculated by the VMEC equilibrium code is $R = 4.55$ m, where the iota is 1.5. The iota is equivalent to inverse of the safety factor q. Since $T_e = 0.3$ keV at $R = 4.55$ m, the real boundary may be slightly outside. The cutoff surfaces of probe microwaves with the frequency of 61.81 GHz and 63.01 GHz are close to the equilibrium boundary.

Figure 12 shows A, I, and Q of MIR signals of 63.01 GHz, which corresponds to the cutoff density at $R = 4.54$ m. Figure 13 shows color contour plot of A when EHO appears. Here, horizontal and vertical axis are pixel numbers in the toroidal and poloidal directions of HMA, respectively. Each pixel corresponds to 2 cm in the plasma. This image frame corresponds to about 10 × 14 cm in the toroidal and poloidal

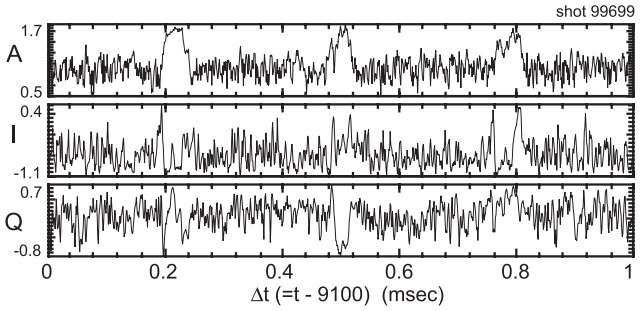

FIG. 12. Raw signal of MIR in the case of high density plasma.

directions in the plasma. RF1, RF2, RF3, and RF4 correspond the illumination frequencies, 60.41, 61.81, 63.01, and 64.61 GHz, respectively. White broken line indicates direction of magnetic field lines. Δt is defined as $\Delta t = t - 9100$ ms and log scale is used for the amplitude A. Sensitivity of each pixel has not calibrated yet.

A narrow red region along the field line can be seen in the images of RF1, RF2, and RF3 during EHO, as shown in Fig. 13. The width of this structure is 5 cm and the thickness is 2 cm in the radial direction. This structure is localized at the surface of iota = 1.5 in this case. Considering the averaged minor radius is 60 cm, the poloidal width of this structure is 2% of the plasma circumference. This narrow structure corresponds to the pulse train with the period of 0.3 ms in the A signal, as shown in Fig. 12. The period of pulse train is consistent with the frequency of EHO. However, this structure is not seen in the image of RF4 in Fig. 13, while EHO is observed in any channel of RF4. EHO is often observed in the standard operation of LHD, but this structure is rarely observed. Therefore, this structure is not EHO, but is associated with EHO. Probably, this structure would be a localized MHD mode that

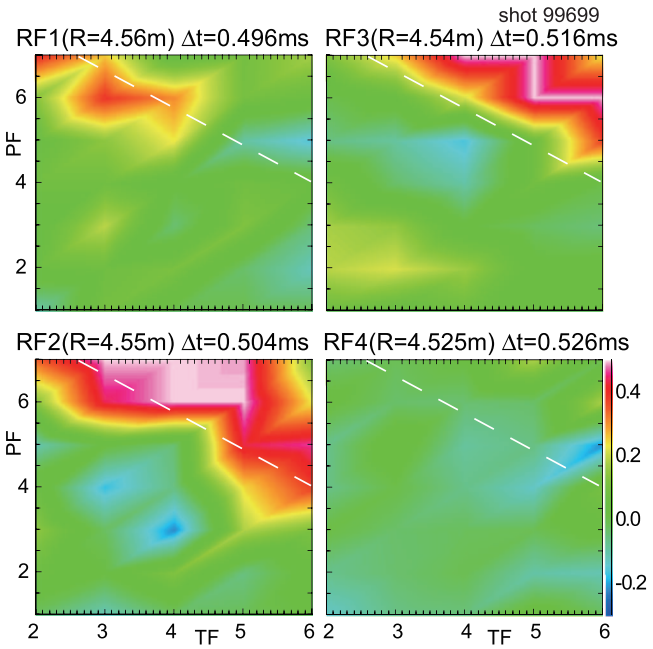

FIG. 13. 2D MIR images of narrow structure associated with EHO on four reflection layers. Here white broken line indicates direction of magnetic field lines, and $\Delta t = t - 9100$.

is induced by EHO. However, the occurrence condition of this narrow structure has not been identified yet.

VI. CONCLUSION

In conclusion, 3D MIR diagnostics has been developed in LHD. The imaging optics and 2D horn antenna array make 2D image and four frequency probe beam and receivers provide radial profiles. The optical system consists of aluminum mirrors and a slant vacuum window in order to minimize disturbance due to spurious reflections. By using 3D MIR, edge plasma dynamics such as EHO has been observed in LHD. A narrow structure along the field line has been found during EHO. This structure may be an MHD mode which is induced by the EHO.

ACKNOWLEDGMENTS

The authors would like to thank Professor S. Sudo, Professor K. Kawahata, Professor H. Hojo, and Professor H. Yamada for the help and encouragement to carry out this work. The work is supported by Grant-in-Aid for Scientific Research (Grant No. 21246140), National Institute for Fusion Science (NIFS) (Grant Nos. KEIN1111 and ULPP008) and National Institute of Natural Sciences (NINS) Imaging Science Project (Grant No. KNSI001).

[1]Y. Nagayama, S. A. Sabbagh, J. Manickam, E. D. Fredrickson, M. Bell, R. V. Budny, A. Cavallo, A. C. Janos, M. E. Mauel, K. M. McGuire, G. A. Navratil, G. Taylor, and M. Yamada, Phys. Rev. Lett. **69**, 2376 (1992).
[2]E. Mazzucato, Nucl. Fusion **41**, 203 (2001).
[3]S. Yamaguchi, Y. Nagayama, R. Pavlichenko, S. Inagaki, Y. Kogi, and A. Mase, Rev. Sci. Instrum. **77**, 10E930 (2006).
[4]S. Yamaguchi, Y. Nagayama, Z. Shi, R. Pavlichenko, S. Inagaki, Y. Kogi, and A. Mase, J. Plasma Fusion Res. **2**, S1038 (2007).
[5]S. Yamaguchi, Y. Nagayama, D. Kuwahara, T. Yoshinaga, Z. B. Shi, Y. Kogi, and A. Mase, Rev. Sci. Instrum. **79**, 10F111 (2008).
[6]T. Munsat, E. Mazzucato, H. Park, B. H. Deng, C. W. Domier, N. C. Luhmann, Jr., J. Wang, Z. G. Xia, A. J. H. Donne, and M. van del Pol, Rev. Sci. Instrum. **74**, 1426 (2003).
[7]B. H. Deng, C. W. Domier, N. C. Luhmann, Jr., D. L. Brower, G. Cima, A. J. H. Donne, T. Oyevaar, and M. J. van de Pol, Rev. Sci. Instrum. **72**, 301 (2001).
[8]Y. Nagayama, S. Yamaguchi, Z. Shi, Y. Kogi, A. Mase, S. Sugito, Y. Hirano, S. Kiyama, H. Koguchi, H. Sakakita, K. Yambe, and N. Ohyabu, J. Plasma Fusion Res. **3**, 053 (2008).
[9]Z. B. Shi, Y. Nagayama, S. Yamaguchi, D. Kuwahara, T. Yoshinaga, S. Sugito, Y. Hirano, H. Koguchi, S. Kiyama, H. Sakakita, K. Yambe, and C. Michael, Phys. Plasmas **18**, 102315 (2011).
[10]D. Kuwahara, S. Tsuji-Iio, Y. Nagayama, T. Yoshinaga, Z. Shi, S. Yamaguchi, M. Sugito, Y. Kogi, and A. Mase, J. Plasma Fusion Res. SERIES **8**, 649 (2009).
[11]D. Kuwahara, S. Tsuji-Iio, Y. Nagayama, T. Yoshinaga, Z. Shi, S. Yamaguchi, M. Sugito, Y. Kogi, and A. Mase, J. Plasma Fusion Res. SERIES **9**, 125 (2010).
[12]T. Yoshinaga, Y. Nagayama, D. Kuwahara, H. Tsuchiya, S. Yamaguchi, Y. Kogi, S. Tsuji-Iio, and A. Mase, Rev. Sci. Instrum. **81**, 10D915 (2010).
[13]T. Yoshinaga, D. Kuwahara, Y. Nagayama, H. Tsuchiya, S. Yamaguchi, Y. Kogi, S. Tsuji-Iio, H. Hojo, and A. Mase, J. Plasma Fusion Res. **5**, 030 (2010).
[14]D. Kuwahara, S. Tsuji-Iio, Y. Nagayama, T. Yoshinaga, H. Tsuchiya, S. Sugito, S. Yamaguchi, Y. Kogi, K. Akaki, and A. Mase, Rev. Sci. Instrum. **81**, 10D919 (2010).
[15]Y. Nagayama, T. Yoshinaga, D. Kuwahara, S. Yamaguchi, Y. Hamada, N. Ito, Y. Ito, Y. Kogi, A. Mase, Z. B. Shi, S. Sugito, H. Tsuchiya, S. Tsuji-Iio, and LHD Experimental Group, J. Soc. Plasma, Fusion **87**, 359 (2011) (in Japanese).
[16]N. Ito, A. Mase, Y. Kogi, Z. Shen, N. C. Luhmann, Jr., N. Seko, M. Tamada, and E. Sakata, J. Plasma Fusion Res. **2**, S1042 (2007).
[17]H. Hojo, R. Kurosawa, and A. Mase, Rev. Sci. Instrum. **70**, 983 (1999).
[18]Y. Kogi, T. Sakoda, A. Mase, N. Ito, S. Yamaguchi, Y. Nagayama, and K. Kawahata, J. Plasma Fusion Res. **2**, S1032 (2007).
[19]C. M. Greenfield, K. H. Burrell, J. C. DeBoo, E. J. Doyle, and B. W. Stallard *et al.*, Phys. Rev. Lett. **86**, 4544 (2001).
[20]T. Oishi, S. Kado, and M. Yoshinuma *et al.*, Phys. Plasmas **13**, 104504 (2006).